

# Instance attack: an explanation-based vulnerability analysis framework against DNNs for malware detection

Ruijin Sun<sup>1</sup>, Shize Guo<sup>2</sup>, ChanYou Xing<sup>1</sup>, YeXin Duan<sup>3</sup>, LuMing Yang<sup>4</sup>, Xi Guo<sup>Corresp., 5</sup>, ZhiSong Pan<sup>Corresp. 1</sup>

<sup>1</sup> Army Engineering University of PLA, Nanjing, China

<sup>2</sup> National Computer Network and Information Security Management Center, Beijing, China

<sup>3</sup> Army Military Transportation University of PLA, zhenjiang, China

<sup>4</sup> National University of Defense Technology, Changsha, China

<sup>5</sup> University Of Science and Technology Beijing, Beijing, China

Corresponding Authors: Xi Guo, ZhiSong Pan

Email address: xiguo@ustb.edu.cn, hotpzs@hotmail.com

Deep Neural Networks (DNNs) are increasingly being used in malware detection and their robustness has been widely discussed. Conventionally, the development of an adversarial example generation scheme for DNNs involves either detailed knowledge concerning the model (i.e., gradient-based methods) or a substantial quantity of data for training a surrogate model. However, under many real-world circumstances, neither of these resources is necessarily available. Our work introduces the concept of the instance-based attack, which is both interpretable and suitable for deployment in a black-box environment. In our approach, a specific binary instance and a malware classifier are utilized as input. By incorporating data augmentation strategies, sufficient data are generated to train a relatively simple and interpretable model. Our methodology involves providing explanations for the detection model, which entails displaying the weights assigned to different components of the specific binary. Through the analysis of these explanations, we discover that the data subsections have a significant impact on the identification of malware. In this study, a novel function preserving transformation algorithm designed specifically for data subsections is introduced. Our approach involves leveraging binary diversification techniques to neutralize the effects of the most heavily-weighted section, thus generating effective adversarial examples. Our algorithm can fool the DNNs in certain cases with a success rate of almost 100%. Instance attack exhibits superior performance compared to the state-of-the-art approach. Notably, our technique can be implemented in a black-box environment and the results can be verified utilizing domain knowledge. The model can help to improve the robustness of malware detectors.

# 1 Instance Attack: An Explanation-based 2 Vulnerability Analysis Framework Against 3 DNNs for Malware Detection

4 Sun RunJin<sup>1</sup>, Guo ShiZe<sup>2</sup>, Xing ChangYou<sup>1</sup>, Duan YeXin<sup>4</sup>, Yang LuMing<sup>3</sup>,  
5 Guo xi<sup>5</sup>, and Pan ZhiSong<sup>1</sup>

6 <sup>1</sup>Army Engineering University of PLA

7 <sup>2</sup>National Computer Network and Information Security Management Center

8 <sup>3</sup>National University of Defense Technology

9 <sup>4</sup>Army Military Transportation University of PLA

10 <sup>5</sup>University Of Science & Technology Beijing

11 Corresponding author:

12 Pan ZhiSong, Guo Xi

13 Email address: hotpzs@hotmail.com, xiguo@ustb.edu.cn

## 14 ABSTRACT

15 Deep Neural Networks (DNNs) are increasingly being used in malware detection and their robustness has  
16 been widely discussed. Conventionally, the development of an adversarial example generation scheme  
17 for DNNs involves either detailed knowledge concerning the model (i.e., gradient-based methods) or a  
18 substantial quantity of data for training a surrogate model. However, under many real-world circumstances,  
19 neither of these resources is necessarily available. Our work introduces the concept of the instance-  
20 based attack, which is both interpretable and suitable for deployment in a black-box environment. In our  
21 approach, a specific binary instance and a malware classifier are utilized as input. By incorporating  
22 data augmentation strategies, sufficient data are generated to train a relatively simple and interpretable  
23 model. Our methodology involves providing explanations for the detection model, which entails displaying  
24 the weights assigned to different components of the specific binary. Through the analysis of these  
25 explanations, we discover that the data subsections have a significant impact on the identification of  
26 malware. In this study, a novel function preserving transformation algorithm designed specifically for  
27 data subsections is introduced. Our approach involves leveraging binary diversification techniques to  
28 neutralize the effects of the most heavily-weighted section, thus generating effective adversarial examples.  
29 Our algorithm can fool the DNNs in certain cases with a success rate of almost 100%. Instance attack  
30 exhibits superior performance compared to the state-of-the-art approach. Notably, our technique can be  
31 implemented in a black-box environment and the results can be verified utilizing domain knowledge. The  
32 model can help to improve the robustness of malware detectors.

## 33 INTRODUCTION

34 Malware attack is an important issue in today's cybersecurity community. Thousands of malware attacks  
35 are reported every day, according to (Demetrio et al., 2021a)'s description. Both academia and industry  
36 have devoted a lot of manpower to malware detection. Traditional detection methods, such as SVM  
37 (Li et al., 2015) and signature (Vinod et al., 2012) require manual feature engineering, which can be a  
38 daunting task. Given the vast number of malware instances in existence, the labor-intensive nature of this  
39 work renders it both time-consuming and tedious. As DNNs have made significant advances in many  
40 domains, such as image (Sharif et al., 2016) and voice classification (Qin et al., 2019), an increasing  
41 number of researchers and anti-virus enterprises have begun leveraging DNN-based detectors in the field  
42 of cybersecurity. The DNNs models automatically make the classification for malware without expert  
43 knowledge. Researchers use deep learning models in an end-to-end manner that operates directly on the  
44 raw bytes of Windows Portable Executable (PE) files.

45 In the domain of cybersecurity, malware detection systems can be broadly classified into dynamic and

46 static approaches. While dynamic systems rely on learning the behavioral features of malware for  
47 classification, static systems directly classify files using features without executing them (Sharif et al.,  
48 2019). This paper primarily focuses on the static approach. There exist several byte-based deep neural  
49 network (DNN) models that have demonstrated comparable performance with traditional methods (Saxe  
50 and Berlin, 2015)(Raff et al., 2018). The robustness of the DNNs detection system and the interpretability  
51 of DNNs have attracted much attention, while the DNNs have shown great potential. The interpretability  
52 of models is particularly important in financial and security-related domains. The absence of model  
53 interpretability can significantly limit the applicability of DNN models in these domains. Adversarial  
54 examples are the techniques that focus on perturbing the examples to mislead DNN-based detection  
55 systems, and can be leveraged to enhance the robustness of such systems. Unlike other domains, semantic  
56 invariance constraints must be satisfied in binary. When an adversarial example is generated, its characters  
57 may be transformed and its semantic should not be changed. People introduce different transformation  
58 techniques that could keep the functionality of the binaries intact (Anderson et al., 2018)(Song et al.,  
59 2020)(Park et al., 2019). In the context of binary-based adversarial attacks, transformations refer to  
60 modifications made to a Windows Portable Executable (PE) file that do not alter the execution of its  
61 underlying code (Anderson et al., 2018). Despite the considerable progress that has been made in  
62 generating adversarial examples for malware detection, there are still a number of unresolved issues. First,  
63 only a few articles that use DNNs to detect malware have explained their detection models. The lack of  
64 transparency makes it questioned by many people (Arp et al., 2022). The uninterpretable model may  
65 detect the binaries according to false causalities that are unrelated to any malicious activity (Arp et al.,  
66 2022). Second, the binary transformation methods used by others focus on the structural part (Demetrio  
67 et al., 2021a) and the code part (Sharif et al., 2019), but they leave the data section alone. Third, after  
68 figuring out how to transform malware, they resort to complicated optimization methods (such as genetic  
69 algorithms) (Demetrio et al., 2021a) or uninterpretable stochastic methods (Sharif et al., 2019). These  
70 deficiencies limit their performance under the black-box model. Our approach fills the gap.  
71 In this paper, we propose the notion of instance-based attacks. Our method is very similar to the transfer-  
72 based approach. The most important difference between instance-based and transfer-based methods is  
73 that all the data used to train our model is generated by data augmentation from one single binary. We use  
74 an explanation based adversarial example generation technique to test malware detectors by iteratively  
75 approximating the decision boundary. Our method is more effective than others in the context of black-box  
76 settings. In order to evade the DNNs in fewer steps, we could transform the most influential modules  
77 in each round. Furthermore, our optimization method is interpretable and can be verified with domain  
78 knowledge. We highlight our contributions below.

- 79 • We introduce the concept of the instance-based attack. Rather than training a surrogate model  
80 against the entire model, we instead train a surrogate model for an instance, with a specific  
81 emphasis on perturbing around that instance. The adversarial instances are generated by iteratively  
82 approximating the decision boundary.
- 83 • Several prominent detection models are analyzed using a local interpretable model, their char-  
84 acteristics and drawbacks are highlighted. Notably, we observed a lack of focus on data section  
85 transformations within PE files, representing a significant gap in current approaches.
- 86 • A novel functionality-preserving transformation method is proposed which is suitable for data  
87 sections in PE files that have not been evaluated by other authors.
- 88 • The theoretical and mathematical foundations of our model are discussed.
- 89 • Our method are tested in various scenarios, and the results demonstrate its superiority over other  
90 state-of-the-art approaches in black-box settings (Sharif et al., 2019). It can achieve a success rate  
91 of almost 100% in certain cases.

## 92 **BACKGROUND AND RELATED WORK**

93 In this section, we provide an overview of the most commonly used DNN-based malware detection  
94 models, with a particular emphasis on their static components. Following this, adversarial methods  
95 designed to target the raw bytes of PE files in malware detectors are discussed. Finally, we conclude the  
96 section by examining literature that explains the use of DNNs for malware classification.

### 97 **DNNs for Malware Detection**

98 Malware detection plays an important role in the field of cyber security. DNNs have been used widely by  
99 researchers in malware classification. The most appealing aspect of the DNNs-based malware detectors is  
100 their ability to achieve state-of-the-art performance from raw bits rather than manually crafted features that  
101 require tedious human effort. Many DNNs-based detectors have been proposed so far, and we introduce  
102 the most famous ones here. Nataraj et al. (2011) visualize the malware binaries as gray-scale images. A  
103 classification method using standard image features is proposed, based on the observation that malware  
104 images belonging to the same family appear very similar in layout and texture. Then they use the classifier  
105 originally designed for images to sort malware. Coull and Gardner (2019) introduce a DNN with five  
106 convolutional and pooling layers. It also has a learnable 10-dimensional embedding layer. At the end  
107 of the network, there is a single fully-connected layer and a sigmoid function. Saxe and Berlin (2015)  
108 employ four distinct complementary features from the static, benign and malicious binaries. They use  
109 a DNNs-based classifier which consists of an input layer, two hidden layers, and an output layer. They  
110 translate the output of the DNNs into a score that can be realistically interpreted as an approximation of  
111 the probability that the file is malware. Johns (2017) proposes deep convolutional neural networks (CNN)  
112 that combine a ten-dimensional, learnable embedding layer with a series of five interleaved convolutional  
113 and max-pooling layers arranged hierarchically. MalConv (Raff et al., 2018) is the most popular CNN  
114 model which combines an eight-dimensional trainable embedding layer. Raff et al. (2018) have tried  
115 many different structures. They have tried deeper networks (up to 13 layers), narrower convolutional  
116 filters (width 3–10), and smaller strides (1–10). Finally, they adopted the network consisting of two 1-D  
117 gated convolutional windows with 500 strides. We used the MalConv detection model to evaluate the  
118 effectiveness of our method.

### 119 **Adversarial Examples Against DNN-based Malware Detectors**

120 Adversarial examples are the technologies that focus on the minimal input perturbations of break machine  
121 learning algorithms. They can expose the vulnerability of the machine learning model and improve the  
122 robustness of the DNNs. For example, when DNNs are used in street sign detection, researchers show  
123 ways to mislead street signs recognition (Chen et al., 2019). Adversarial examples could also fool voice-  
124 controlled interfaces (Qin et al., 2019), mislead NLP tasks (Jia and Liang, 2017). It is natural to introduce  
125 adversarial sample techniques to bypass DNNs based malware detectors. However, the semantics of  
126 binaries limit the applicability of the existing adversarial methods designed against image, voice, or  
127 NLP classifiers transplanted to the cybersecurity realm, because there is a structural interdependence  
128 between adjacent bytes. Anderson et al. (2018) introduce one way to bypass machine-learning-based  
129 detection by manipulating the PE file format. They find several structures in Windows PE files that could  
130 be modified without affecting their functionality. Kreuk et al. (2018) craft bytes adversarially in regions  
131 that do not affect execution. Specifically, they append adversarial bits at the end of files. Suciú et al.  
132 (2019) extend this idea by finding more places to append in PE files, such as in the middle of two sections  
133 of PE files. Different padding strategies are also evaluated, including random appending, FGM appending,  
134 and benign appending. Sharif et al. (2019) manipulate instructions to produce adversarial examples.  
135 Instructions are a functional part of binary files. They introduce two families of transformations. The first  
136 one named in-Place randomization (IPR) is quoted from (Pappas et al., 2012). The second one named code  
137 displacement (Disp) is also adopted in our article as the baseline. Disp relocates sequences of instructions  
138 that contain gadgets from their original locations to newly allocated code segments with a *jmp* instruction.  
139 Sharif et al. (2019) extend the Disp algorithm. They make it possible to displace any length of consecutive  
140 instructions, not just those belonging to gadgets. As far as the variable space is concerned, they focus on  
141 the structure characteristic or the code characteristic. None of the above-mentioned articles discuss the  
142 data segment, although it plays an important role in malware classification.

### 143 **Explanation of Adversarial Machine Learning in Malware**

144 In the field of malware, the traditional routine for producing adversarial examples in black-box settings  
145 involves proposing function-preserving actions and using a uninterpretable method (Anderson et al., 2018)  
146 or a random method (Sharif et al., 2019) to evade DNNs. Different ways are presented to transform  
147 malware without changing its functionality, but only a few articles have explained why their approaches  
148 work. Due to the non-linearity of DNNs detectors, they rely on uninterpretable methods or random ways  
149 to optimize their transformation. These methods are of little help in designing the malware detector.  
150 Demetrio et al. (2021a) use the genetic algorithm to generate the adversarial examples. Sharif et al. (2019)

151 use the transformation randomly. Anderson et al. (2018) use DNNs based reinforcement learning to evade  
152 the detector which is also uninterpretable. While DNNs have shown great potential in various domains, the  
153 lack of transparency limits their application in security or safety-critical domains. Arp et al. (2022) claim  
154 that artefacts unrelated to the classified target may create shortcut patterns to separate different classes.  
155 Consequently, the DNNs may adapt to the artefacts instead of the original problems. It is important to  
156 investigate what these models have learned from malware. An interpretable technique is needed to tell us  
157 the most influential features. Most of the existing research on the interpretability of DNNs focuses on  
158 image classification and NLP processing (Ribeiro et al., 2016)(Camburu, 2020)(Lundberg and Lee, 2017).  
159 To improve the transparency of malware classification, researchers have started to work on the explanation  
160 issue of malware classification. To the best of our knowledge, Coull and Gardner (2019) are the first  
161 to explore this topic. They use various methods such as hdbscan, shaply value and byte embeddings to  
162 analyze the model. They examine the learned features at multiple levels of resolution, from individual  
163 byte embeddings to end-to-end analysis of the model. Jeffrey Johns et al. also examine what DNNs  
164 have learned in malware classification by analyzing the activation of the CNN filter. They suggest that a  
165 CNN-based malware detector could find meaningful features of malware (Johns, 2017). Luca Demetrio's  
166 work is the closest one to our research. They use Integrated Gradients to find the most important input and  
167 point out that the MalConv model does not learn the key information in the PE file header according to  
168 the interpretability analysis (Demetrio et al., 2019). They devise an effective adversarial scheme based on  
169 the explanation. Rosenberg et al. (2020) make use of the explainable techniques to train a surrogate neural  
170 network to represent the attacked malware classifier. They attack the surrogate model instead. Different  
171 from these articles, our function-preserving measures are able to process more types of segments and  
172 fewer examples are needed.

## 173 TECHNICAL APPROACH

174 In this section, we discuss the technical approach behind our framework. First, the general algorithm is  
175 described. Then, we introduce the approximating boundary model for fitting the DNNs. Next, the data  
176 augmentation module are present. Finally, how we create adversarial examples are explained in detail.  
177 Throughout the paper, we use the following notations.  $m$  refers to the original malware,  $f(m)$  refers to  
178 the output of the DNNs detector (e.g. class probabilities or logits). We use  $g(m) = \vec{m} \circ \vec{w}$  to approximate  
179  $f(m)$ .  $\vec{m}$  is the interpretable data representation vector.  $\vec{w}$  is the weight of the linear equation.  $\tilde{m}^i$  refers to  
180 the perturbed malware in the  $i$ -th round of the algorithm and  $\tilde{m}_j^i$  is the  $j$ -th perturbed example in each  
181 round.  $r_j$  is the perturbation that we make.

### 182 Instance Attack

183 Portions of this text were previously published as part of a preprint (RuiJin et al., 2022). In the field of  
184 adversarial examples for binary code in a black-box setting, the transformation can only be limited to a  
185 few discrete actions as mentioned in Section:Function Invariant Transformation because of the semantic  
186 invariance constriction. The transformation is discrete and difficult to optimize with gradient-descent  
187 methods. Therefore, interpretable models are being exploited to make adversarial attacks. Adversarial  
188 attacks can roughly be divided into three categories: gradient-based, transfer-based, and score-based (or  
189 decision-based) attacks (Brendel et al., 2018). Our method is somewhat similar to the transfer-based  
190 method. Traditionally a transfer-based method trains a surrogate neural network model on a training set  
191 that is believed to accurately represent the attacked malware classifier such as (Rosenberg et al., 2020). To  
192 train a surrogate model, traditional methods require a large number of examples. This is often impossible  
193 in practice. The framework for training our surrogate model is distinct from other models in that it only  
194 requires a single sample to be trained. Our framework fits a specific example, not the detection model. To  
195 accomplish this, we train a surrogate model that is designed to precisely represent the specific instance  
196 being fitted. A locally interpretable algorithm is used in training the surrogate model. For example, for a  
197 DNN detector  $f$  and a malware  $m_0$ , we can train a surrogate model  $g(m_0^1) = f(m_0^1), g(m_0^2) = f(m_0^2), \dots$ .  
198 But for another malware  $n$ ,  $g(n_0) \neq f(n_0)$ .  
199 A locally generated linear function  $g$  is used to find the important features of the binary, then the function  
200 invariant transformation mentioned in Section:Function Invariant Transformation is used to remove the  
201 features. Since only one binary is required, we name it Instance Attack.

## 202 General Framework

203 Our model works in a black-box setting. We assume that we have no access to the model parameters and  
 204 the data set. We don't have any idea about the structure of the classification model and the distribution  
 205 of the data set. Only one binary instance is given. There is no limit to the number of queries. We can  
 206 transform the instance arbitrarily. Our target is to generate a new binary to mislead the classifier. After the  
 207 transformation, we have to guarantee the functionality of the program.

208 The basic intuition of our framework is to approximate the result of the specific example with a linear  
 209 function and make the perturbation towards the approximate decision boundary iteratively. The whole  
 210 procedure works in rounds, where each round consists of three steps. In the first step, data augmentation  
 211 is used to generate a large number of new samples from the original binary. Then a linear model is used to  
 212 fit these samples. Here, the FastLSM algorithm will be used (described in detail in Section: Interpretable  
 213 Data Representations and Segmentation Algorithm) to fit the malware detector  $f$  with a linear function  
 214  $g$ . The second step is to approximate the decision boundary by solving the linear equations  $g = benign$ ,  
 215 and transforming the most important part of the malware accordingly to make  $g(\tilde{m}^i) = benign$ . For the  
 216 function invariant restriction of the binary file,  $\tilde{m}^i$  is transformed to  $\tilde{m}^{i+1} = \tilde{m}^i + r^i$  with the function  
 217 invariant transformation we propose in Section: Function Invariant Transformation. We finally query the  
 218 black-box detector to get  $f(\tilde{m}^{i+1})$ . If the result of  $f(\tilde{m}^{i+1})$  is still malware, we move on to the next  
 219 iteration or we stop the algorithm if the maximum number of iterations is reached. Algorithm 1 shows the  
 pseudocode of the whole procedure.

---

### Algorithm 1 General algorithm

**INPUT:** a malware  $m$ , a classifier  $f$ , a linear equation  $g$ , the approximation algorithm  $FastLSM()$ , a  
 functional invariant transformation function  $Tran()$ , address of most weighted data  $[start, end]$

**OUTPUT:** a new malware  $\tilde{m}^i$

```

1: while  $i < maxiteration$  do
2:    $g(\tilde{m}^i) \leftarrow FastLSM(\tilde{m}^i, f())$ 
3:    $start, end \leftarrow solving \quad g(\tilde{m}^i) = benign$ 
4:    $\tilde{m}^{i+1} \leftarrow Tran(start, end, \tilde{m}^i)$ 
5:   if  $f(\tilde{m}^{i+1}) == malware$  then
6:      $i \leftarrow i + 1$ 
7:   else
8:     return success
9:   end if
10: end while
11: return false
```

---

220

## 221 How Interpretability Is Applied

222 In traditional detection models, the initial step involves selecting features, followed by designing the  
 223 detection algorithm. In contrast, DNNs are end-to-end models, they eliminate the need for explicit feature  
 224 extraction. They can directly input raw data into the model and learn the desired outcomes. DNNs are  
 225 often referred to as featureless models due to their ability to learn features internally. Similarly, existing  
 226 attack models that target DNNs do not possess knowledge of the feature weights. These attack models  
 227 launch direct attacks without this crucial information. While direct attacks may occasionally be successful,  
 228 they fail to provide insights into understanding deep detection models. In contrast, our approach focuses  
 229 on acquiring the features employed in deep detection models or identifying the associated feature weights.  
 230 By modifying features with higher weights, we aim to achieve the attack objective. We utilize the instance  
 231 attack model to calculate the weights of different parts (superpixels) within the binary. If a superpixel  
 232 possesses a high weight in this model and is associated with code segments or data segments, we proceed  
 233 with targeted attacks. These steps are iterated, resulting in the displacement of superpixels. Through  
 234 this process, we are able to gain insights into the functioning of the DNN model and effectively execute  
 235 targeted attacks.

### 236 Formalizing The Model

237 Adversarial examples are variants of normal examples by adding some imperceptible perturbations. The  
 238 adversarial examples cause the detection model to misclassify examples with high confidence. Carlini  
 239 and Wagner (2017) model the adversarial examples as a constrained minimization problem:

$$\min D(\tilde{m}^i, \tilde{m}^{i+1}) \quad (1)$$

$$s.t \quad f(\tilde{m}^{i+1}) = benign \quad (2)$$

240  $\tilde{m}^i$  is fixed and the object is to find the perturbation  $\tilde{m}^{i+1}$  that can minimize  $D(\tilde{m}^i, \tilde{m}^{i+1})$  and further leads  
 241 to the evasion.  $D(\tilde{m}^i, \tilde{m}^{i+1})$  is a distance function and the perturbation is subject to  $f(\tilde{m}^{i+1}) = benign$ .  
 242 Since the identifier is a black-box model, it is difficult to find a solution for the original function  $f$ . Carlini  
 243 and Wagner (2017) proposed to solve a simple objective function  $G$  instead,  $G(\tilde{m}^{i+1}) = benign$  if and  
 244 only if  $f(\tilde{m}^{i+1}) = benign$ .

$$\min D(\tilde{m}^i, \tilde{m}^{i+1}) \quad (3)$$

$$s.t \quad G(\tilde{m}^{i+1}) = benign \quad (4)$$

245 In malware detection, these formulas are also utilized to find adversarial perturbations  $\tilde{m}^{i+1}$  for the  
 246 original binary  $\tilde{m}^i$  that target a class  $f_{benign}$ . In a black-box environment, finding an object function  $G$   
 247 such that  $G(\tilde{m}^{i+1}) = benign$  if and only if  $f(\tilde{m}^{i+1}) = benign$  is an overly strong requirement. Here the  
 248 local explanation  $g$  is used instead. If  $f(\tilde{m}^{i+1}) = benign$  is true, then  $g(\tilde{m}^{i+1}) = benign$  is established, but  
 249 the opposite is not necessarily true. When  $g(\tilde{m}^{i+1}) = benign$  is true,  $f(\tilde{m}^{i+1})$  may not be  $benign$ . The  
 250 optimization could be converted to the following problem:

$$\min D(\tilde{m}^i, \tilde{m}^{i+1}) \quad (5)$$

$$s.t \quad g(\tilde{m}^{i+1}) = benign \quad (6)$$

251 Eq. (6) can easily be solved to get the minimal perturbation  $r$  from  $\tilde{m}^i$  to  $\tilde{m}^{i+1}$ , since  $g$  is a linear equation.  
 252 Because  $g(\tilde{m}^i + r)$  is the approximation of  $f(\tilde{m}^{i+1})$ , we must incorporate the perturbation  $\tilde{m}^{i+1}$  back into  
 253 the original classifier  $f$  to get the accurate value. If  $f(\tilde{m}^{i+1}) = benign$ , then we stop the algorithm or  
 254 we should recompute the linear approximation of  $f(\tilde{m}^{i+1})$ . We continue to repeat this process until the  
 255 evasion is successful or the maximum number of iterations is reached.

### 256 Local Linear Explanations of Malware Detection

Here, how we build the linear function  $g$  are explained. Our method is inspired by Local Interpretable  
 Model-Agnostic Explanations(LIME) (Ribeiro et al., 2016) and Locally Linear Embedding (LLE) (Roweis  
 and K.Saul, 2000). Deep learning algorithms provide highly satisfactory results. However, their decision  
 procedures are non-linear and the important parts of the input data cannot be featured out directly. When  
 one instance are given to bypass the classifier, we try to infer how the detector behaves around a specific  
 instance by querying the detector for the results of different transformed examples. The data augmentation  
 method are used to produce the adversarial perturbations. As claimed in (Roweis and K.Saul, 2000), it is  
 assumed that binary files can be represented by points in a high-dimensional vector space. The binary and  
 its transformations lie on or close to the locally linear path of the manifold. In this context, it is assumed  
 that the coherent structure between the binary and its variants leads to strong correlations, which can be  
 characterized by linear coefficients. The use of a linear model is considered simple and interpretable, as it  
 allows for a clear understanding of the relationship between the different features of the binary and its  
 variants.

$$\xi(m) = \operatorname{argmin}_{g \in G} \mathcal{L}(f, g, \Pi_m) + \Omega(g) \quad (7)$$

257 Eq. (7) describes how to solve this problem, where  $f$  denotes a DNNs detector, and  $g$  is an interpretable  
 258 model to approximate  $f$  without knowing its parameters. In classification,  $f(m)$  produces the probability  
 259 (or a malware indicator) that  $m$  belongs to a certain category. If  $g$  is a potentially interpretable function,  
 260 and  $\Omega(g)$  measures the complexity of the explanation.  $\mathcal{L}(f, g, \Pi_m)$  measures how unfaithful  $g$  is  
 261 in approximating  $f$  in the locality defined by  $\Pi_m$ . To ensure the interpretability and local closeness,  
 262  $\mathcal{L}(f, g, \Pi_m)$  should be minimized and  $\Omega(g)$  should be low enough. The lower the  $\Omega(g)$ , the easier it

263 is for humans to understand the model. In this paper,  $G$  could be the class of linear models, such that  
 264  $g(m) = \vec{w}_g \circ \vec{m}$ . It is stated that an interpretable representation  $\vec{m}$  of  $m$  can be obtained directly, the specific  
 265 rule is described in the following section. it is defined that  $\Pi_m(\vec{m}_i^t) = D(\vec{m}_i^t, \vec{m}_0^t)$ , where  $D$  is some kind of  
 266 distance function, for example, the  $L2$ -norm distance.  $\vec{m}_0^t$  is the specific example and  $\vec{m}_j^t$  is the perturbed  
 267 example in each round. We carefully choose some perturbed examples  $\vec{m}_1^t, \vec{m}_2^t, \vec{m}_3^t \dots, \vec{m}_j^t$  within each  
 268 round. For information on the method of perturbation, see Section:Data Augmentation Module.  $\mathcal{L}$  could  
 269 be a locally weighted square loss as defined in Eq. (9). In this way, the function has been converted into a  
 270 linear function fitting problem.

$$g(\vec{m}_j^t) = \vec{w}_i \circ \vec{m}_j^t \quad (8)$$

$$\mathcal{L}(f, g, \Pi_m) = \sum_j \Pi_m(\vec{m}_j^t) (f(\vec{m}_j^t) - g(\vec{m}_j^t))^2 \quad (9)$$

271 Given a malware instance  $\vec{m}^t$  and  $f$ , this problem is a typical ordinary least square problem. It is suggested  
 272 that examples around  $\vec{m}^t$  can be sampled by drawing non-zero elements uniformly at random to get the  
 273 value of  $\vec{m}_j^t$ .  $f(\vec{m}_j^t)$  could be obtained by querying the classifier.  $\vec{m}_j^t$  is the interpretable data representation  
 274 that can be easily calculated. By solving these functions, the weight  $\vec{w}_i$  can be obtained for sample  $i$ .  $g$  is  
 275 the local explanation model of  $f$ .  $g$  could also be used as the approximate function of  $f$ .

## 276 Data Augmentation Module And Optimization Algorithm

### 277 Data Augmentation Module

278 Ablation analysis is often used in evaluating the DNNs model. It is a technique for evaluating machine  
 279 learning models by discarding certain features (everybodywiki, 2020). We adopt similar ideas by  
 280 discarding certain features of the instance. As our model is instance-based, we do not quantify the DNNs  
 281 detector, but the important portion of a specific instance. Augmented examples are created from a given  
 282 instance by discarding (masking) certain features. Then a linear function  $g$  is used to fit the DNNs around  
 283 these examples, and the weights for each feature are calculated. Computing the weights of all the bits  
 284 is time-consuming. Given a file of length  $LM$ , it would take  $o(LM^3)$  time to find the most important bit  
 285 using the Least Square Method. To improve efficiency, two optimization mechanisms are proposed. First,  
 286 the superpixel are used as the basic unit of interpretable representation. Then, the FastLSM algorithm are  
 287 introduced to reduce the computational complexity.

### 288 Interpretable Data Representations and Segmentation Algorithm

289 Superpixels were used in image segmentation originally (Ghosh et al., 2019). Common image segmenta-  
 290 tion algorithms include quick shift, felzenszwalb, slic. In this paper, superpixels are the results of a binary  
 291 file over segmentation. We could use the tools to disassemble the binary file, such as IDA, Binary ninja.  
 292 Superpixels are the basic function blocks returned by disassembly tools. The Capstone disassembler  
 293 framework are used in our experiment (Capstone, 2021). A basic block is a straight-line sequence of  
 294 codes with only one entry point and only one exit. Or the examples could just be segmented by their offset.  
 295 For example, a large binary file of size 200KB could be divided into ten parts, each of which would be  
 296 20KB in size. As shown in Figure 1, there are 3 superpixels returned by the disassembly tool. The staed rt  
 297 offsets of these superpixels are 0x10004675h, 0x1000469Ah, and 0x100046A1h. The lengths of the three  
 298 superpixels are 0x25h, 0x7h, and 0x8h respectively. Interpretable data representations  $\vec{m}$  and data features  
 299  $m$  are different. Features  $m$  in the range  $m \in R^L$  are the ground truths. An interpretable representation  $\vec{m}$   
 300 is a binary vector indicating the “presence” (denoted by  $\mathbf{1}$ ) or “absence” (denoted by  $\mathbf{0}$ ) of a patch of  
 301 codes and its range is  $\vec{m} \in \{0, 1\}^l$ .  $L$  is the length of the features and  $l$  is the length of the interpretable  
 302 representations. Given a file whose content is “0x1122”, “0x11” and “0x22” are the two super pixels  
 303 and “11” is their interpretable representation.  $f(“0x1122”) is equal to  $g(“0x1122”) = w_1 * 1 + w_2 * 1$ .  
 304 Sampling around a specific offset in a binary file, such as ”0x1122”, can help to generate the correspond-  
 305 ing interpretable representation of the data. For example, if “0x1122” is transformed to “0x0022”, its  
 306 interpretable representation is transformed to “01”. Table 1 shows the examples in detail.$

### 307 Fast Least Square Method

308 In Algorithm 1 referred, it is necessary to find the minimum perturbation at each round. Sometimes the  
 309 weight of the top- $k$  important superpixels is needed instead of each superpixel. Fleshman et al. (2018)  
 310 introduce a segmentation algorithm to find the most important superpixels. We extend it and combine it

```

10004675 loc_10004675:                                ; CODE XREF: DllInstall+8f
10004675                                ; DllInstall+107j
10004675    cmp     [ebp+binInstall], 0
10004679    mov     ecx, offset dword_10014334
1000467E    jz     short loc_100046A1
10004680    push   esi
10004681    push   1
10004683    call   sub_10004520
10004688    mov     esi, eax
1000468A    test   esi, esi
1000468C    jns   short loc_1000469A
1000468E    push   1
10004690    mov     ecx, offset dword_10014334
10004695    call   sub_10004580
1000469A    loc_1000469A:                                ; CODE XREF: DllInstall+9f
1000469A    mov     eax, esi
1000469C    pop     esi
1000469D    pop     ebp
1000469E    retn   8
100046A1 ; -----
100046A1 loc_100046A1:                                ; CODE XREF: DllInstall+2f
100046A1    push   1
100046A3    call   sub_10004580
100046A8    pop     ebp
100046A9    retn   8

```

**Figure 1.** An Example of Superpixels.

Interpretable Representation	00	01	10	11
Original Feature	0x0000	0x0022	0x1100	0x1122

**Table 1.** An example of interpretable data representation.

311 with our local explanation algorithm. It is named as the Fast Least Square Method (FastLSM), because it  
 312 can reduce the computational complexity to  $o(\log(LM))$  to compute the weight of the most important  
 313 superpixel.

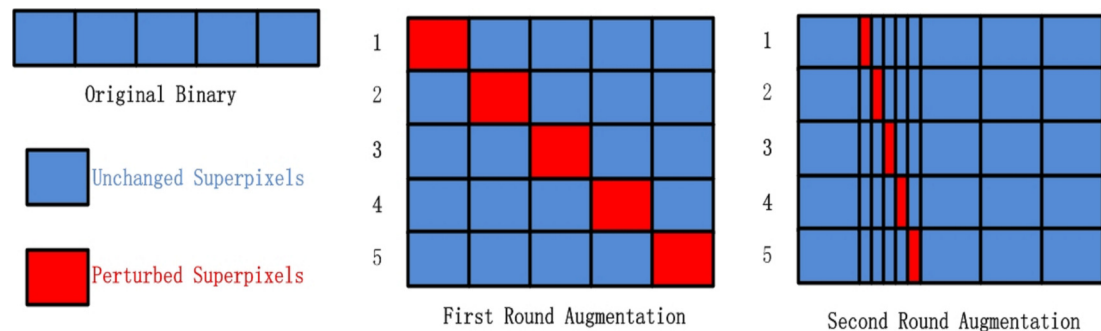


**Figure 2.** The data augmentation algorithm used in our experiments.

314 The steps of FastLSM are as follows. The entire binary are selected as the base superpixel. First, the  
 315 superpixel are divided into  $n$  different superpixels. each super pixel is occluded respectively with zero  
 316 to generate variants and each variant is analyzed by the DNNs  $f$ . Second, we choose the variant that  
 317 results in a larger drop in classification confidence. Third, if the length of the superpixel with a larger  
 318 drop is smaller than a specific value  $\beta$ , it is set as the base superpixel and the algorithm starts over from  
 319 the beginning. There are different ways to occlude the superpixel. This can be done by replacing it  
 320 with random values, null values, or adversarial values (Fleshman et al., 2018). We will discuss how to  
 321 determine the hyperparameter  $\beta$  in Chapter 4.6. Figure 2 illustrates the overarching process of FastLSM,  
 322 depicting the general flow and steps involved in the algorithm. The Algorithm 2 provides a comprehensive  
 323 breakdown of the fundamental stages comprising FastLSM, elucidating the specific actions and operations  
 324 undertaken within the algorithmic framework.  
 325

**Algorithm 2** FastLSM algorithm

**INPUT:** a malware  $m$ , a classifier  $f$ , a target occlusion size  $\beta$ ,  $n$  is the number of segments within each iteration

**OUTPUT:** a new malware  $\tilde{m}$

- 1: Split file  $m$  into  $n$  sections,  $splitsize \leftarrow \lfloor m \div n \rfloor$ , size of  $i$ th section is  $|m(i)| = splitsize$
- 2: Use LSM to get the weight for each section
- 3: Find the  $j$ th section with the maximum weight
- 4:  $start \leftarrow$  start address of  $j$ th section
- 5:  $end \leftarrow$  end address of  $j$ th section
- 6: **while**  $splitsize > \beta$  **do**
- 7:      $max \leftarrow 1, i \leftarrow 1$
- 8:     **while**  $i < n$  **do**
- 9:          $starttemp \leftarrow (start + splitsize * (i - 1))$
- 10:          $endtemp \leftarrow (start + splitsize * i)$
- 11:          $m_i[starttemp:endtemp] \leftarrow 0x00$ , occlusion the  $i$ th segment with 0x00
- 12:          $starttemp \leftarrow (start + splitsize * (max - 1))$
- 13:          $endtemp \leftarrow (start + splitsize * max)$
- 14:          $m_{max}[starttemp:endtemp] \leftarrow 0x00$ , occlusion the most weight segment with 0x00
- 15:         **if**  $f(m_i) < f(m_{max})$  **then**
- 16:              $max \leftarrow i$
- 17:              $i \leftarrow i + 1$
- 18:         **else**
- 19:              $i \leftarrow i + 1$
- 20:         **end if**
- 21:     **end while**
- 22:      $start \leftarrow start + splitsize * (max - 1)$ .
- 23:      $end \leftarrow start + splitsize * (max)$ .
- 24:      $splitsize \leftarrow splitsize \div n$
- 25: **end while**
- 26: **return**  $\tilde{m}[start : end]$

326 **Function Invariant Transformation**

327 The semantics of binaries hinder the direct transplantation of existing traditional adversarial learning  
 328 methods. Even changes as small as one bit can disrupt the original syntax of the binary and may cause it  
 329 to malfunction or even crash. For example, if the characters are changed from **53** to **52** in the binary file,  
 330 at the assembly level it means that **push ebx** is changed to **push edx** and the function of the generated  
 331 adversarial example would be invalid. Because of the function preserving constraint, the transformations  
 332 that we use are limited to those that preserve the function of the binary. In this paper, three families of  
 333 transformations are used. The first transformation is an appending algorithm that applies the evasion  
 334 by appending adversarial bits at the end of the original files (Suciu et al., 2019). These bytes cannot  
 335 affect the semantic integrity. Appending bytes to inaccessible regions of the binary may be easy to  
 336 detect and could be sanitized statically (Sharif et al., 2019). The second transformation that we use  
 337 is named code displacement (Disp), which was proposed by (Koo and Polychronakis, 2016) to break  
 338 the gadgets originally. Sharif et al. (2019) adopt it to mislead DNNs-based classifiers. The general  
 339 idea of Disp is to move some codes to the end of the binary. The original codes are replaced by a *jmp*  
 340 instruction at the beginning of the code segment. After filling the newly allocated code segment with  
 341 the adversarial codes, another *jmp* instruction is immediately appended. The third transformation is an  
 342 original one named data displacement (DataDisp). Disp can only transform code segments rather than  
 343 data segments. However, we find that the DNNs sometimes attach importance to data segments as shown  
 344 in the experiment (Section:Distribution). Therefore, we propose DataDisp, an algorithm that could be  
 345 used to transform data segments (this transformation can also be applied to code segments with some  
 346 modifications). DataDisp is a practical code diversification technique for stripped binary executables.  
 347 DataDisp transfers data to the end of the file and uses the *mov* instruction to move the data back before  
 348 the binary is executed. It starts by adding a new section at the end of the PE file. The original codes  
 349 to be moved are replaced with adversarial data (Fleshman et al., 2018), random data, or null data. After

350 filling the newly allocated segment with the *mov* code, a *jmp* instruction is immediately appended to give  
 351 control back to the original binary. At last, the OEP are changed to the beginning of the newly allocated  
 352 section. There are a few tips to be noted. If the displaced codes contain important structural information  
 (e.g., **edata** section) we leave them alone.

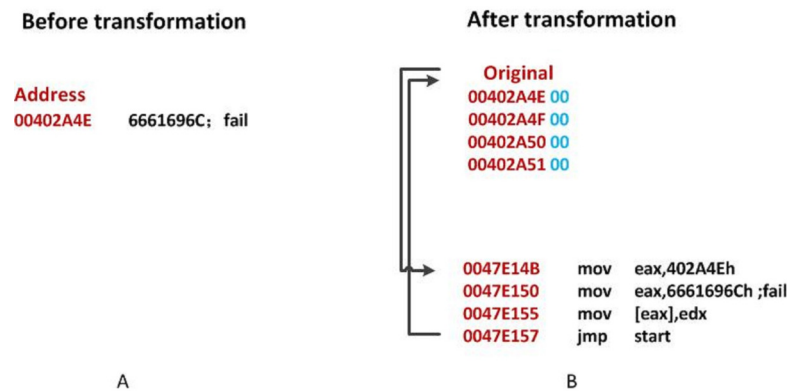


**Figure 3.** An illustration of DataDisp transformation.

353 As shown in Figure 3a, the original data at 0x402A4E is the string *fail*, and is replaced by 0x00. The  
 354 Original Entry Point (OEP) address is displaced to 0x47E14B in Figure 3b. Then the address 0x402A4E  
 355 is stored in *EAX*. The new code will reconstruct the original file using *mov*. After the reconstruction, it  
 356 will *jmp* back to the original OEP.  
 357

## 358 EVALUATION

359 This section presents comprehensive empirical evidence for the adversarial theme. First, we describe the  
 360 datasets and the DNN detectors in detail. We also discuss the interpretational analysis on the experimental  
 361 data. Then, different methods of transformations are presented. Finally, our model is compared with three  
 362 other methods. The results demonstrate that our adversarial example generation model is trustworthy.

### 363 Datasets and Malware Detector

Class	All	Train	Validation	Test
Malware	10868	8708	1080	1080
Benign	9814	7814	1000	1000

**Table 2.** The number of binaries for training, validating and testing the DNNs.

364 All experiments were conducted on an Ubuntu 18.04 server with an Intel Xeon CPU and 64GB of  
 365 RAM. The computer was equipped with Python 3.7, PyTorch, and an NVIDIA GTX3090 Graphics  
 366 processing unit. A mixed data set is used. We resorted to a publicly available dataset to collect malware.  
 367 And benign binaries are collected by ourselves. The malware binaries were adopted from the Kaggle  
 368 Microsoft Malware Classification Challenge (Ronen et al., 2018). This dataset contains nine different  
 369 families of malware. Even though there are no benign ones, we still used the dataset to train our model. It  
 370 is based on the following considerations. First, most previous works (Anderson and Roth, 2018)(Krčál  
 371 et al., 2018)(Raff et al., 2018) used proprietary datasets and some other public datasets contain only  
 372 packed data (Vigna and Balzarotti, 2018). The dataset of (Noever and Miller.Noever, 2021) contains only  
 373 processed data. Although Yang et al. (2021) also offer sufficient raw files, they do not provide benign  
 374 files either, for copyright reasons. Second, over fifty articles had cited this dataset (Ronen et al., 2018),  
 375 which was the de facto standard for malware classification. Our dataset of benign binaries was collected  
 376 from a newly created Windows 7 machine. We used two specific tools, **Portable apps** and **360 package**  
 377 **manager**, to install a total of 180 different packages. To ensure that our dataset was representative, we

Classifier	Accuracy		
	Train	Validation	Test
MalConv	98.8%	97.8%	96.1%
AvastNet	99.8%	97.2%	97.5%

**Table 3.** The DNN's performance

378 also included popular files such as Chrome, Firefox, and notepad++. In addition, we collected packages  
 379 that were likely to be used by academics (such as MiKTeX and MATLAB), developers (such as VSCode  
 380 and PyCharm), and document workers (such as WPS and Adobe Reader). By including a diverse range of  
 381 packages, our dataset provides a comprehensive representation of commonly used software across various  
 382 domains. We selected 9,814 benign binaries, most of them were smaller than 2MB. The files are divided  
 383 into the train, validation, and test sets as shown in Table 2.

384 Two DNN classifiers were chosen from those mentioned in Section: BACKGROUND AND RELATED  
 385 WORK. Both classifiers were given raw byte binaries. The first classifier, named AvastNet, is a four-layer  
 386 convolutional neural network with four fully connected layers. It receives inputs of up to 512KB and was  
 387 proposed by (Krčál et al., 2018). The second DNN model is called MalConv and was proposed by (Raff  
 388 et al., 2018). Its network structure consists of two 1-D gated convolutional windows with 500 strides,  
 389 and it receives inputs of up to 2MB. To evaluate the performance of these models, we split all the files  
 390 into three sets: training, test, and validation. Both of these DNNs achieved accuracies above 95% on our  
 391 datasets. The classification results of these two DNNs are shown in Table 3.

392 Because there were no PE headers in the Microsoft dataset, disassembling the binaries to validate our  
 393 algorithm was not possible. Consequently, we turned to **VirusShare** and downloaded malware samples  
 394 from the nine malware families that were not present in the Microsoft dataset. VirusShare is an open  
 395 repository of malware samples with labels. We obtained 88 binaries that belonged to the same nine  
 396 families but did not appear in the training set. These samples are then evaluated against MalConv and  
 397 AvastNet separately. The results are shown in Table 4, where 68 of them were identified as malware by  
 398 MalConv. We also sampled 88 benign binaries for the test, 10 of which were misclassified by MalConv.  
 399 AvastNet marked 72 of them as malware, as shown in Table 4. We also sampled 88 benign binaries for  
 400 testing, 8 of which were misclassified by AvastNet.

Class	Model	all	as malicious	as benign
Malware	MalConv	88	77.3%	22.7%
Benign	MalConv	88	11.4%	88.6%
Malware	AvastNet	88	81.2%	18.8%
Benign	AvastNet	88	9.1%	90.9%
Malware	Endgame	88	87.5%	12.5%
Benign	Endgame	88	5.7%	94.3%

**Table 4.** Binaries used to test our model.

401 In addition to the two DNNs that we trained, we evaluated our attacks using a publicly available  
 402 model Endgame(Anderson and Roth, 2018). It is a gradient boosed decision tree (GBDT) model using  
 403 LightGBM with default parameters (100 trees, 31 leaves per tree), resulting in fewer than 10K tunable  
 404 parameters. The dataset of Endgame includes features extracted from 1.1M binary files: 900K training  
 405 samples (300K malicious, 300K benign, 300K unlabeled). As there is no raw file available in Endgame  
 406 dataset, we turned to **VirusShare**. For our evaluation, we utilized the identical set of 176 binaries that  
 407 were previously tested in MalConv and Avast to assess the performance of the Endgame model. Out of  
 408 these 88 malware binaries, Endgame successfully identified 77 of them as malware. Additionally, we  
 409 included 88 benign binaries in our test set, out of which Endgame erroneously misclassified 5 as malware.

410 **Weight Analysis On Superpixels**  
 411 ***Distribution***

Weight	[0,0.01]	[0.01,0.1]	[0.1,0.2]	[0.2,1]
MalConv	43.2%	50.8%	5.5%	0.5%
AvastNet	44.2%	50.2%	5.2%	0.4%

**Table 5.** Percentage of superpixels with different weights.

412 We used the least square algorithm to obtain the weights of different parts of the binaries and con-  
 413 ducted a statistical analysis to understand the black-box classifier. The sampled files were divided into  
 414 superpixels that were smaller than 8KB and larger than 4KB, and we summarized the corresponding  
 415 weights of these superpixels for the MalConv and AvastNet classifiers. As shown in Table 5, 90% of the  
 416 superpixels had a weight of less than 0.1, and only about 5% of the superpixels were between 0.1 and 0.2.  
 417 0.5% of the superpixels had a weight greater than 0.2. We can even estimate their distribution. We plot the  
 418 weight of different superpixels of the malware on MalConv, as shown in Figure 4. In general, although  
 419 the sum of the weights of all the superpixels must be greater than 0, the weight distribution conforms  
 420 to the normal distribution, and the mean is approximately zero. Figure 4 shows the result of the weight  
 421 analysis on MalConv, and the analysis on AvastNet looks similar.

According to the weight distribution diagram, we can conclude that most of the contents have little

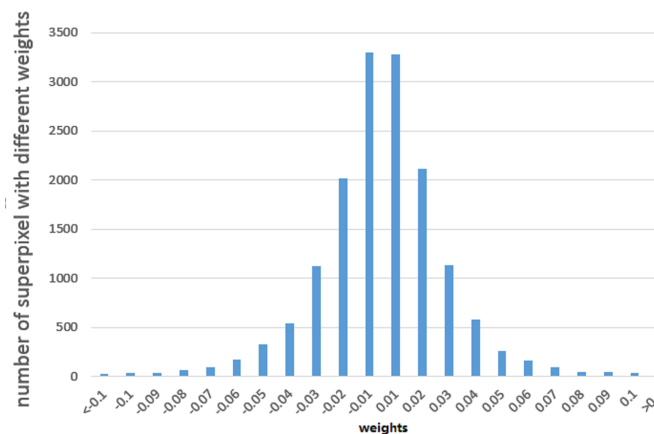


**Figure 4.** Weight distribution diagram under the MalConv classifier. It shows that the weight distribution curve of the malware follows the normal distribution.

422 influence on the result. There are only less than one percent of the superpixels that have a significant  
 423 impact on the classifier, whose weight is greater than 0.2. We could use the data as adversarial data in the  
 424 following experiments. Some superpixels with higher absolute weight are listed below. The data that is  
 425 shown in Figure 5b has a negative impact on the MalConv classifier. It's a URL for **digicert.com**. This  
 426 website is obviously not malicious. The presence of these codes in binaries can increase the probability of  
 427 being classified as benign. The data in Figure 5a plays positively to AvastNet, this figure is the disassembly  
 428 result of IDA Pro. We can see that the code is the **import table** of a PE file. Many of the functions in the  
 429 table are related to malicious behavior with high probabilities, such as the **isdebuggerpresent** which is  
 430 the API that is often used by malware to resist reverse analysis.  
 431

432  
 433 We also analyzed the malware containing malicious APIs with the lightGBM model Endgame which  
 434 is introduced by (Anderson and Roth, 2018). The lightGBM model was not trained on the same dataset  
 435 as our model. Although the output of lightGBM was 0.8388964 which implied that there was a high  
 436 probability that the file was malware. But by analyzing the file with our interpretable model, we can see



**Figure 5.** Data with different weights. The data on the right (b) has a positive impact on the results. The data on the left (a) has a negative effect.

437 that the model gave most weight to the file's PE header. We show the weight and offset of the three most  
 438 weighted superpixels in Table 6. We could conclude that the lightGBM model makes decisions according  
 439 to the header features.

Offset	0x0000-0x1000	0xe000-0xf000	0xc000-0xd000
Weight	0.93	-0.0277	-0.0272

**Table 6.** The weight and offset of the three most weighted superpixels of the malware under the lightGBM. 0x0000-0x1000 is the address of the PE header. The model gave too much weight to the file's PE header, we concluded that the lightGBM model makes a decision according to false causalities.

440

#### 441 **Proportion of Code Segment Weight**

442 We also examined the proportion of code segments in the total score generated by the classifiers. To  
 443 analyze the results, we employed an explanation-based model. The weight of the code segments are  
 444 calculated by adding the weight of all the superpixels that belonged to the code segments. Although it was  
 445 not strictly defined, it corresponded to the code/text section of the binaries (Microsoft, 2021). However,  
 446 the author of the malware could change the name of the code segment at will. By using the explanation  
 447 model, we could get the weight of all the sections (bss, edata, idata, idlsym, pdata, rdata, reloc, rsrc, sbss,  
 448 sdata, srdata, code/text). We computed the weight of code/text for all binaries and presented the CDF in  
 449 Figure 6. The CDF reveals that the weight of code sections amounts to roughly 50% in half of all the  
 450 binaries. Although this was only an estimation, the weight of the code segments must be limited. We  
 451 concluded that code sections only account for part of the weight. Due to the fact that not all data segments  
 452 can be transformed by Disp, it is highly probable that the success rate will be low if the Disp algorithm is  
 453 used alone.

#### 454 **Randomly Applied Transformations**

455 In order to study the influence of the location of the transformed content and the type of the transformed  
 456 content on the success rate of adversarial examples, we evaluated whether the randomly applied transfor-  
 457 mation would lead to evasion of the DNNs. To evaluate the transformations, we created up to 200 variants  
 458 for each binary. If the detection results of more than one variant changed, the transformation would be  
 459 considered successful. The binary are divided into superpixels. For code sections, the superpixel was  
 460 the basic functional block returned by the disassembly tools. For data sections, we divided binaries into  
 461 1KB length superpixels by offset. The concept of "randomly applied transformations" encompassed two  
 462 aspects. Firstly, whether a particular superpixel in the binary underwent transformation was determined  
 463 randomly. Secondly, the gap space following the transformation was filled either with adversarial data  
 464 or random data. Specifically, we designed two experiments. We conducted two distinct experiments to

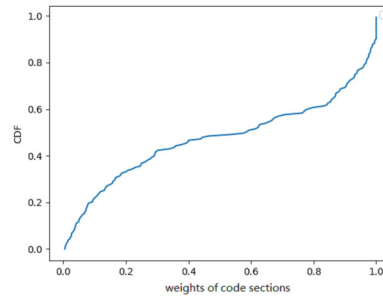


**Figure 6.** A cumulative distribution function (CDF) graph depicting the weight of code sections contributing to the decision provides valuable insights into the behavior of a malware detection model. Approximately 50% of the binary's code sections have little contribution to the final result.

465 test our approach. In the first experiment, we filled the gap spaces with random data, while in the second  
466 experiment, we used adversarial data to fill the gaps. The adversarial data was the data we found in the  
467 previous section with a high absolute weight.

468 We conducted both experiments with the constraint that the size of each binary would not increase by  
469 more than 5%, and limited the number of iterations to 200 for both Disp and DataDisp. When Disp and  
470 DataDisp were both used randomly with random data, the results showed that three malware binaries  
471 were misclassified, and five benign binaries were incorrectly classified as malware when using MalConv.  
472 4 malware and 6 benign binaries were misclassified for AvastNet. The results are easy to explain under  
473 our framework, because the weight is under a normal distribution with a mean value of 0 as shown in  
474 Figure 4. If the Disp&DataDisp algorithms are applied randomly, the weight of the transformed binaries  
475 is also under a normal distribution and the sum of the weights has a high probability with a mean value  
476 of 0. There is a high probability that the adversarial examples will not evade the detector. So we could  
477 conclude that it's not that the DNNs are robust against naive Disp transformations as claimed in (Sharif  
478 et al., 2019) but it's just a matter of probability. However, when we filled the gap spaces with adversarial  
479 data, the results improved significantly. The adversarial data was selected from the higher-weighted data  
480 we identified in the previous section. Using this approach, we achieved a success rate of 24% for MalConv  
481 and 39% for AvastNet, which represented the highest success rates obtained in our experiments.

#### 482 **Evaluation of the Transformations: Disp and DataDisp**

483 In this section, we evaluated the Disp and DataDisp transformations individually using an interpretable  
484 model to optimize the procedure. With regards to Disp, we set the maximum displacement budget to  
485 5% and the maximum number of iterations to 200. We filled the gap left by the transformation with  
486 adversarial data. The Disp algorithm could achieve a maximum success rate of 59% for MalConv and  
487 45% for AvastNet. With regards to DataDisp, we used a maximum displacement budget of 5% and a  
488 maximum number of iterations of 200. Once again, we filled the gap spaces left by the transformation  
489 with adversarial data. The DataDisp algorithm yielded a maximum success rate of 53% for MalConv and  
490 35% for AvastNet.

491 Sharif et al. (2019) also tested Disp with a hill-climbing approach. They only moved subsections that had  
492 a positive impact on the results. They got a maximum success rate of 24%. Our hypothesis was that this  
493 result was due to the fact that Disp was only capable of transforming the code section of a binary file.

#### 494 **Evaluation On Explanation-Based Adversarial Algorithm**

495 In this subsection, we evaluated our explanation-based model by comparing it to other algorithms. We  
496 set the maximum displacement budget to 5% and limited the number of rounds to 200. To improve the  
497 performance, we used a combination of Disp and DataDisp transformations. We compared our model  
498 with three different models, they were Disp with a hill-climbing approach (Sharif et al., 2019), genetic  
499 padding (Demetrio et al., 2021a) and gradient-based attack (Kreuk et al., 2018). All of these algorithms,  
500 including the explanation-based model, increased the length of the binary by padding different contents at  
501 the end of the file. The gradient-based algorithm operated in a white-box setting, using the parameters of

502 the DNNs to calculate the gradient (Suciu et al., 2019)(Kreuk et al., 2018). The gradient-based padding  
 503 we used was adapted from (Kreuk et al., 2018) with epsilon 0.5 and iteration 2. The genetic padding was  
 504 a black-box approach that we adapted from (Demetrio et al., 2021a) with iteration 10 and population 50.  
 505 The genetic padding required data randomly sampled from different files. Similar to the genetic padding  
 506 algorithm, our approach also worked in a black-box setting. However, we improved upon this method  
 507 by adding binary files with the most weighted data identified in the previous section. The impact of this  
 508 modification can be seen in the results displayed in Figure 7.

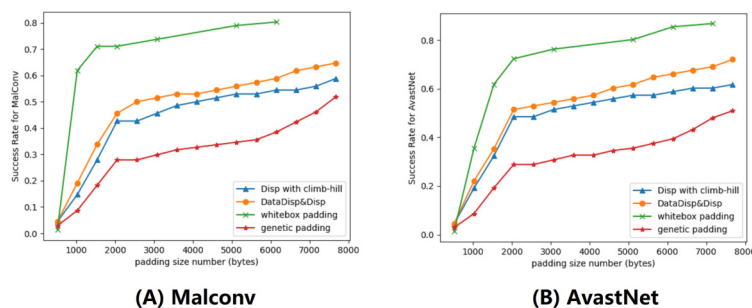


**Figure 7.** We provided a demonstration of various attacking algorithms, where the orange line represents the misclassification rate of our black-box algorithm. Our approach proved to be less effective than the gradient-based algorithm, but outperformed both genetic padding and Disp in combination with the climb-hill algorithm within a certain range.

509 Although our algorithm was not as effective as the gradient-based model, we observed that it outper-  
 510 formed genetic padding and Disp with the hill-climbing approach. Notably, the gradient-based attack  
 511 requires model information that may be unavailable in practice. Among all black-box models, our attack  
 512 model yielded the best performance. However, without budget constraints, our explanation-based model  
 513 could result in a much higher number of misclassified binaries. To comprehensively evaluate our attack  
 514 model, we also conducted attacks on the Endgame model. The results demonstrate a maximum success  
 515 rate of 52%. The Endgame model, which benefits from a larger training dataset, incorporates substantial  
 516 structural information in its features. These features, unfortunately, are immutable in our attack model,  
 517 consequently resulting in the relatively poorer performance of our attacks.

## 518 Computational Analysis

519 In our paper, we evaluated the performance of our attack on three different models: MalConv and Avast,  
 520 which are DNN-based models, and the Endgame model, which is a gradient boosted decision tree model.  
 521 The DNN models have a linear complexity when it comes to training, as it depends on the length of the  
 522 binary input. On the other hand, the complexity of the Endgame model is determined by the number of  
 523 trees and the number of leaves per tree. It is important to note that none of these models were developed  
 524 by us, so we focused on analyzing the computation requirements for generating adversarial examples. The  
 525 complexity of the attack model consists of two parts: the time required to displace instructions and the  
 526 time required to query the detector. Displacing instructions randomly within a binary function with  $k$   
 527 instructions has a time complexity of  $o(k)$ . If the length of the binary function is  $n$ , the query time is  
 528  $o(\log(n))$  time complexity. For the instance attack model, the overall running time of the model is equal  
 529 to the sum of query time and the time to displacing the instructions, which is  $o(\log(n) + k)$ . Regarding  
 530 the collected data on actual running conditions, there were 1805, 1921 query for attacking MalConv and  
 531 Avast on average. The attacks took 630, 730 seconds on average respectively for Malconv and Avast  
 532 model. The average number of queries was 6210 with an average time of 1545s for Endgame.

## 533 Miscellaneous

534 **Hyperparameters.** Throughout this article, we chose 200 as the maximum number of iterations and 5%  
 535 as the maximum displacement budget, we also used 1KB as the size of the superpixel of DataDisp in  
 536 Section:Randomly Applied Transformations. We used these hyperparameters because our method could

537 achieve almost perfect success under this configuration. In (Sharif et al., 2019)(Lucas et al., 2021), they  
538 tested Disp with a hill-climbing approach with similar hyperparameters.

539 **Integrity of binary.** To ensure that the functionality of the binaries was intact after the transformation.  
540 Firstly, we selected 6 different binaries and manually checked their instructions with OllyDbg (Oleh  
541 Yuschuk, 2014). Secondly, we selected 10 different benign binaries and manually checked their function-  
542 ality by running them on Windows. All the files worked fine. Thirdly, we also used the Cuckoo Sandbox  
543 (Claudio Guarnieri, Alessandro Tanasi, Jurriaan Bremer, and Mark Schloesser, 2019) to test 10 malware  
544 programs. One of them collapsed after transformation, and the rest ones functioned normally. We checked  
545 the file manually. We found that the binary does not strictly follow the PE format specification. The length  
546 of the data segment shown in the file header does not match the actual length.

## 547 **DISCUSSION AND FUTURE WORK**

548 In this section, we presented the results of our experiments and highlighted areas for future improvement.  
549 We also briefly covered the limitations and basic assumptions of our model.

### 550 **Discussion On Experiments**

551 We carefully designed multiple sets of experiments to evaluate the effectiveness of our approach. First,  
552 we analyzed binary files to identify which content the black-box detector valued and used this informa-  
553 tion for targeted attacks. Second, we randomly applied transformations in Section:Randomly Applied  
554 Transformations but found that these techniques alone were not sufficient to achieve high adversarial  
555 results. This demonstrated the importance of both optimization and adoption of adversarial data. Third,  
556 we compared our model with others and observed that it did not perform as well as the gradient-based  
557 attack model. However, it is important to note that the gradient-based model works in white-box settings  
558 and requires model information that may not be available in practice. Our adversarial model utilized  
559 Disp & DataDisp transformation methods to transform both data and code segments, resulting in the best  
560 performance under black-box conditions.

### 561 **Discussion On The Model**

562 In black-box attacks, adversaries lack knowledge of the internal workings of the model. To overcome this,  
563 adversaries may leverage adversarial classifier reverse engineering (ACRE) to learn sufficient information  
564 for recovering the classifier (Lowd and Meek, 2005). Another approach for attacking black-box systems  
565 is to train a substitute model using synthetic inputs generated by adversaries (Szegedy et al., 2014). This  
566 method is based on the assumption that two models with comparable performance solving the same ML  
567 task are likely to have similar decision boundaries (Papernot et al., 2018). We make a similar assumption  
568 that two models with comparable performance around one instance are likely to have similar decision  
569 boundaries. So we train a surrogate model around a specific example. Compared with training a surrogate  
570 model on the entire data set, the instance-based approach greatly reduces the computational complexity of  
571 training and reduces the amount of data required.

572 Our model requires only a single training instance rather than many. In practice, we often have access to  
573 only one or a few examples and need to generate enough targeted adversarial samples. The inputs used  
574 to train the surrogate model are transformed solely from the example itself because a coherent structure  
575 between the binary and its variants leads to strong correlations. We believe that the information learned  
576 from these perturbed instances is specific and targeted. By training a simpler substitute model, we can  
577 then use this model as our target for attack. This approach is referred as the instance-based attack. In  
578 Locally Linear Embedding(LLE) (Roweis and K.Saul, 2000), each data point is a linear combination of its  
579 neighbours. As claimed in LLE (Roweis and K.Saul, 2000), we assume that the binary and its perturbed  
580 instances lie on or close to a locally linear path of the manifold. So we can characterize each binary from  
581 its neighbours by linear coefficients. This is the key assumption of our paper.

582 After discussing the mathematical basis of the instance attack model, we concluded that our fitting function  
583 is necessary but not sufficient. Thus, we must iterate the process many times. Unlike in NLP and image  
584 classification, the goal is not to minimize perturbation but rather to maintain the function's integrity. For  
585 two semantically identical binary files, their characters may have no resemblance to each other. This is  
586 why we need to make many transformations.

### 587 **Limitations and Future Works**

588 Limited by our linear fitting model, our interpretable model is not suitable for some structure-based  
589 adversarial transformations such as content shifting (Demetrio et al., 2021b)(Anderson et al., 2018). Our  
590 algorithm is instance-based, which means that it needs a lot of queries and calculations to do an adjustment  
591 for each example. However, the convergence of the algorithm has not been proven and we have to iterate  
592 many times. We use a linear function to fit the classifier. We believe that we could introduce some more  
593 complex models such as the local non-linear interpretable model (Guo et al., 2018), and the accuracy  
594 can be furtherly improved. The combination of global fitting and local fitting frameworks is also worth  
595 exploring and the intrinsic dimension of our model could also be discussed (Pope et al., 2021). In the  
596 field of malicious code detection, conventional models do not typically impose limitations on the number  
597 of queries, as scanning a single personal computer often necessitates querying millions of files. However,  
598 our model does not possess a distinct advantage in scenarios where query efficiency is paramount. Thus  
599 far, there has been no evident demand for such capabilities in the domain of code analysis. Nevertheless,  
600 exploring avenues to significantly reduce the number of queries on the base of (Guo et al., 2019) remains  
601 a promising research direction.

### 602 **Potential Mitigations**

603 While our model has achieved a commendable success rate, it is crucial to develop mitigation measures  
604 that bolster the resilience of malware detection against potential evasion efforts stemming from our attack  
605 strategies. Although our model necessitates a substantial number of queries for effective implementation,  
606 we do not regard this as an inherently efficacious mitigation approach. Static detection is widely acknowl-  
607 edged as being generally undecidable. However, we posit that the following two techniques can impart a  
608 degree of mitigation against our attack model. Firstly, our model primarily focuses on the perturbation  
609 of code and data segments. By ascribing higher weights to structural elements such as file headers  
610 or structure data entities like input/output functions name, we can augment the accuracy of detection.  
611 Secondly, Our model does not affect the dynamic execution of the code. Through the integration of static  
612 and dynamic detection methodologies, such attack methods can be proficiently circumvented.

### 613 **CONCLUSIONS**

614 Our paper introduces a new concept, known as the "instance-based attack," through which we analyzed two  
615 DNN-based malware classifiers using an interpretable model. Our analysis revealed key characteristics  
616 of these models under black-box conditions, highlighting the critical role played by data segments in  
617 determining results. This importance of data segments had not been discussed in related articles before.  
618 Additionally, we introduced a novel method to generate adversarial examples, which we call the instance  
619 attack. Unlike other methods that insert code in invalid places or transform only code segments, our  
620 adversarial model can transform both data and code segments using Disp and DataDisp. Our model  
621 achieves state-of-the-art results under black-box conditions, and the results of the instance attack can be  
622 verified using domain knowledge. We hope that our work will inspire future research efforts in this area.

### 623 **REFERENCES**

- 624 Anderson, H. S., Kharkar, A., Filar, B., Evans, D., and Roth, P. (2018). Learning to evade static PE  
625 machine learning malware models via reinforcement learning.
- 626 Anderson, H. S. and Roth, P. (2018). EMBER: an open dataset for training static PE malware machine  
627 learning models.
- 628 Arp, D., Quiring, E., Pendlebury, F., Warnecke, A., Pierazzi, F., Wressnegger, C., Cavallaro, L., and  
629 Rieck, K. (2022). Dos and don'ts of machine learning in computer security. In *31st USENIX Security  
630 Symposium (USENIX Security 22)*, Boston, MA. USENIX Association.
- 631 Brendel, W., Rauber, J., and Bethge, M. (2018). Decision-based adversarial attacks: Reliable attacks  
632 against black-box machine learning models.
- 633 Camburu, O. (2020). Explaining deep neural networks.
- 634 Capstone (2021). The ultimate disassembly framework - capstone- the ultimate disassembler. <https://www.capstone-engine.org>. Accessed: 2021-03-31.
- 635  
636 Carlini, N. and Wagner, D. A. (2017). Towards evaluating the robustness of neural networks. In *2017  
637 IEEE Symposium on Security and Privacy (SP)*, pages 39–57.

- 638 Chen, S.-T., Cornelius, C., Martin, J., and Chau, D. H. P. (2019). Shapeshifter: Robust physical adversarial  
639 attack on faster r-cnn object detector. In Berlingerio, M., Bonchi, F., Gärtner, T., Hurley, N., and Ifrim,  
640 G., editors, *Machine Learning and Knowledge Discovery in Databases*, pages 52–68, Cham. Springer  
641 International Publishing.
- 642 Claudio Guarnieri, Alessandro Tanasi, Jurriaan Bremer, and Mark Schloesser (2019). Cuckoo sandbox.  
643 <https://www.cuckoosandbox.org>. Accessed: 2022-2-10.
- 644 Coull, S. E. and Gardner, C. (2019). Activation analysis of a byte-based deep neural network for malware  
645 classification. In *2019 IEEE Security and Privacy Workshops (SPW)*, pages 21–27.
- 646 Demetrio, L., Biggio, B., Lagorio, G., Roli, F., and Armando, A. (2019). Explaining vulnerabilities of  
647 deep learning to adversarial malware binaries.
- 648 Demetrio, L., Biggio, B., Lagorio, G., Roli, F., and Armando, A. (2021a). Functionality-preserving  
649 black-box optimization of adversarial windows malware. *IEEE Transactions on Information Forensics  
650 and Security*, 16:3469–3478.
- 651 Demetrio, L., Coull, S. E., Biggio, B., Lagorio, G., Armando, A., and Roli, F. (2021b). Adversarial  
652 examples: A survey and experimental evaluation of practical attacks on machine learning for windows  
653 malware detection. *ACM Trans. Priv. Secur.*, 24(4).
- 654 everybodywiki (2020). Ablation analysis. [https://en.everybodywiki.com/Ablative\  
655 \\_analysis](https://en.everybodywiki.com/Ablative\_analysis). Accessed: 2021-11-22.
- 656 Fleshman, W., Raff, E., Zak, R., McLean, M., and Nicholas, C. (2018). Static malware detection amp;  
657 subterfuge: Quantifying the robustness of machine learning and current anti-virus. In *2018 13th  
658 International Conference on Malicious and Unwanted Software (MALWARE)*, pages 1–10.
- 659 Ghosh, S., Das, N., Das, I., and Maulik, U. (2019). Understanding deep learning techniques for image  
660 segmentation.
- 661 Guo, C., Gardner, J. R., You, Y., Wilson, A. G., and Weinberger, K. Q. (2019). Simple black-box  
662 adversarial attacks. *CoRR*, abs/1905.07121.
- 663 Guo, W., Mu, D., Xu, J., Su, P., Wang, G., and Xing, X. (2018). Lemna: Explaining deep learning based  
664 security applications. page 364–379.
- 665 Jia, R. and Liang, P. (2017). Adversarial examples for evaluating reading comprehension systems.
- 666 Johannes Plachy (2018). Portable executable file format. [https://blog.kowalczyk.info/  
667 articles/pefileformat.html](https://blog.kowalczyk.info/articles/pefileformat.html). Accessed: 2018-7-26.
- 668 Johns, J. (2017). Representation learning for malware classification. [https://www.fireeye.com/  
669 content/dam/fireeye-www/blog/pdfs/malware-classification-slides.pdf](https://www.fireeye.com/content/dam/fireeye-www/blog/pdfs/malware-classification-slides.pdf).  
670 Accessed: 2020-07-26.
- 671 Koo, H. and Polychronakis, M. (2016). Juggling the gadgets: Binary-level code randomization using  
672 instruction displacement. In *Proceedings of the 11th ACM on Asia Conference on Computer and Com-  
673 munications Security*, ASIA CCS '16, page 23–34, New York, NY, USA. Association for Computing  
674 Machinery.
- 675 Kreuk, F., Barak, A., Aviv-Reuven, S., Baruch, M., Pinkas, B., and Keshet, J. (2018). Adversarial  
676 examples on discrete sequences for beating whole-binary malware detection.
- 677 Krčál, M., Švec, O., Bálek, M., and Jašek, O. (2018). Deep convolutional malware classifiers can learn  
678 from raw executables and labels only.
- 679 Li, W., Ge, J., and Dai, G. (2015). Detecting malware for android platform: An svm-based approach. In  
680 *2015 IEEE 2nd International Conference on Cyber Security and Cloud Computing*, pages 464–469.
- 681 Lowd, D. and Meek, C. (2005). Adversarial learning. In *Proceedings of the Eleventh ACM SIGKDD  
682 International Conference on Knowledge Discovery in Data Mining*, KDD '05, page 641–647, New  
683 York, NY, USA. Association for Computing Machinery.
- 684 Lucas, K., Sharif, M., Bauer, L., Reiter, M. K., and Shintre, S. (2021). Malware makeover: Breaking ml-  
685 based static analysis by modifying executable bytes. In *Proceedings of the 2021 ACM Asia Conference  
686 on Computer and Communications Security*, ASIA CCS '21, page 744–758, New York, NY, USA.  
687 Association for Computing Machinery.
- 688 Lundberg, S. and Lee, S. (2017). A unified approach to interpreting model predictions. volume  
689 abs/1705.07874.
- 690 Microsoft (2021). Pe format. [https://docs.microsoft.com/en-us/windows/win32/  
691 debug/pe-format](https://docs.microsoft.com/en-us/windows/win32/debug/pe-format). Accessed: 2021-03-31.
- 692 Nataraj, L., Karthikeyan, S., Jacob, G., and Manjunath, B. S. (2011). Malware images: Visualization and

- 693 automatic classification. In *Proceedings of the 8th International Symposium on Visualization for Cyber*  
694 *Security, VizSec '11*, New York, NY, USA. Association for Computing Machinery.
- 695 Noever, D. and Miller.Noever, S. E. (2021). Virus-mnist:a benchark malware dataset.
- 696 Oleh Yuschuk (2014). Ollydbg. <https://www.ollydbg.de>. Accessed: 2022-2-10.
- 697 Papernot, N., McDaniel, P., Sinha, A., and Wellman, M. P. (2018). Sok: Security and privacy in machine  
698 learning. In *2018 IEEE European Symposium on Security and Privacy (EuroSP)*, pages 399–414.
- 699 Pappas, V., Polychronakis, M., and Keromytis, A. D. (2012). Smashing the gadgets: Hindering return-  
700 oriented programming using in-place code randomization. In *2012 IEEE Symposium on Security and*  
701 *Privacy*, pages 601–615.
- 702 Park, D., Khan, H., and Yener, B. (2019). Short paper: Creating adversarial malware examples using code  
703 insertion.
- 704 Pope, P., Zhu, C., Abdelkader, A., Goldblum, M., and Goldstein, T. (2021). The intrinsic dimension of  
705 images and its impact on learning.
- 706 Qin, Y., Carlini, N., Goodfellow, I., Cottrell, G., and Raffel, C. (2019). Imperceptible, Robust, and  
707 Targeted Adversarial Examples for Automatic Speech Recognition.
- 708 Raff, E., Barker, J., Sylvester, J., Brandon, R., Catanzaro, B., and Nicholas, C. K. (2018). Malware  
709 detection by eating a whole EXE. *WS-18:268–276*.
- 710 Ribeiro, M. T., Singh, S., and Guestrin, C. (2016). "why should i trust you?": Explaining the predictions  
711 of any classifier. In *Proceedings of the 22nd ACM SIGKDD International Conference on Knowledge*  
712 *Discovery and Data Mining, KDD '16*, page 1135–1144, New York, NY, USA. Association for  
713 Computing Machinery.
- 714 Ronen, R., Radu, M., Feuerstein, C., Yom-Tov, E., and Ahmadi, M. (2018). Microsoft malware classifica-  
715 tion challenge.
- 716 Rosenberg, I., Meir, S., Berrebi, J., Gordon, I., Sicard, G., and David, E. (2020). Generating end-to-end  
717 adversarial examples for malware classifiers using explainability. *CoRR*, abs/2009.13243.
- 718 Roweis, S. T. and K.Saul, L. (2000). Nonlinear dimensionality reduction by locally linear embedding.  
719 *SCIENCE*, 290:2323–2326.
- 720 RuiJin, S., ShiZe, G., JinHong, G., ChangYou, X., LuMing, Y., Xi, G., and ZhiSong, P. (2022). Instance  
721 attack:an explanation-based vulnerability analysis framework against dnns for malware detection.
- 722 Saxe, J. and Berlin, K. (2015). Deep neural network based malware detection using two dimensional  
723 binary program features. pages 11–20.
- 724 Sharif, M., Bhagavatula, S., Bauer, L., and Reiter, M. K. (2016). Accessorize to a crime: Real and stealthy  
725 attacks on state-of-the-art face recognition. In Weippl, E. R., Katzenbeisser, S., Kruegel, C., Myers,  
726 A. C., and Halevi, S., editors, *Proceedings of the 2016 ACM SIGSAC Conference on Computer and*  
727 *Communications Security, Vienna, Austria, October 24-28, 2016*, pages 1528–1540. ACM.
- 728 Sharif, M., Lucas, K., Bauer, L., Reiter, M. K., and Shintre, S. (2019). Optimization-guided binary  
729 diversification to mislead neural networks for malware detection.
- 730 Song, W., Li, X., Afroz, S., Garg, D., Kuznetsov, D., and Yin, H. (2020). Automatic generation of  
731 adversarial examples for interpreting malware classifiers.
- 732 Suciu, O., Coull, S. E., and Johns, J. (2019). Exploring adversarial examples in malware detection. In  
733 *2019 IEEE Security and Privacy Workshops, SP Workshops 2019, San Francisco, CA, USA, May 19-23,*  
734 *2019*, pages 8–14. IEEE.
- 735 Szegedy, C., Zaremba, W., Sutskever, I., Bruna, J., Erhan, D., Goodfellow, I. J., and Fergus, R. (2014).  
736 Intriguing properties of neural networks. In Bengio, Y. and LeCun, Y., editors, *2nd International Con-*  
737 *ference on Learning Representations, ICLR 2014, Banff, AB, Canada, April 14-16, 2014, Conference*  
738 *Track Proceedings*.
- 739 Vigna, G. and Balzarotti, D. (2018). When malware is Packin' heat. In *Enigma 2018 (Enigma 2018)*,  
740 Santa Clara, CA. USENIX Association.
- 741 Vinod, P., Laxmi, V., Gaur, M. S., and Chauhan, G. (2012). Momentum: Metamorphic malware  
742 exploration techniques using msa signatures. In *2012 International Conference on Innovations in*  
743 *Information Technology (IIT)*, pages 232–237.
- 744 Yang, L., Ciptadi, A., Laziuk, I., Ahmadzadeh, A., and Wang, G. (2021). Bodmas: An open dataset for  
745 learning based temporal analysis of pe malware. In *2021 IEEE Security and Privacy Workshops (SPW)*,  
746 pages 78–84.

**747 1 APPENDIX****748 1.1 Windows Portable Executable File Format**

749 The data we use in this article are all Windows PE files and we take advantage of the format characteristics  
750 of the PE files to create adversarial examples. The PE files are derived from the Common Object File  
751 Format (COFF), which specifies how Windows executables are stored on the disk. The main file that  
752 specifies the PE files is winnt.h, related documents can also be found in Microsoft (2021). There are two  
753 types of PE files, one is executable (EXE) file and the other is dynamic link library (DLL) file. They  
754 are almost the same in terms of file format, the only difference is that a field is used to identify whether  
755 the file is an EXE or DLL. Generally, PE files can be roughly divided into different components. They  
756 begin with a MS-DOS header, a Stub and a PE file signature. Immediately following is the PE file header  
757 and optional header. Beyond that, section headers and section bodies follow. A PE file typically has  
758 nine predefined sections named .text, .bss, .rdata, .data, .rsrc, .edata, .idata, .pdata and .debug Johannes Plachy  
759 (2018). Figure 8 depicts a typical exemplification of the structure of a PE file. Some binaries do not need  
760 all of these sections while others may rename or define the section names according to their own needs.  
761 For the alignment reason, the start address of the segment part of PE is often 0x100.

### PE File Format

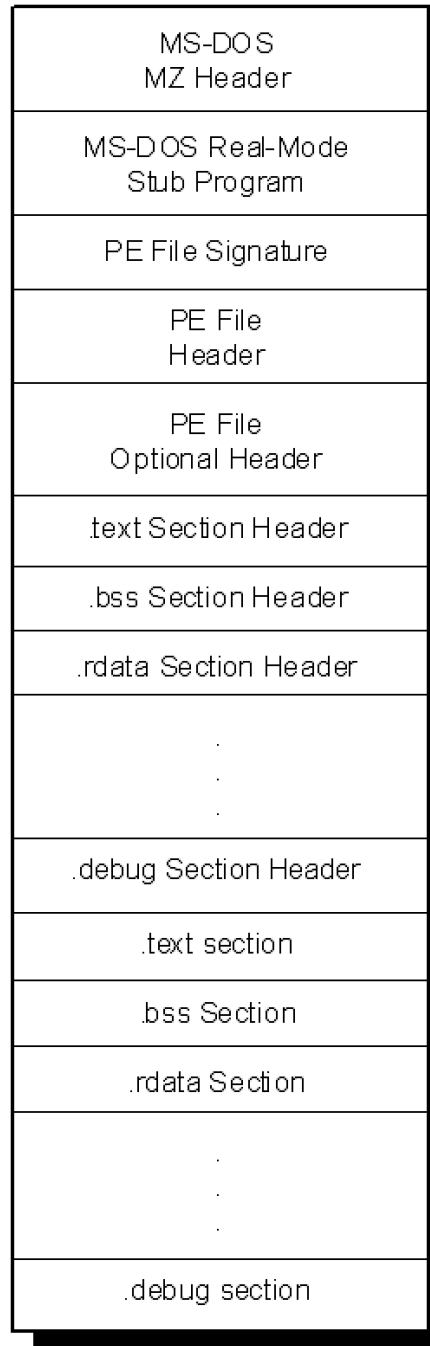


**Figure 8.** Structure of a typical PE file image.